Journal of Materials Chemistry A

RSC Publishing

PAPER

View Article Online
View Journal | View Issue

Boron-doped electrocatalysts derived from carbon dioxide

Cite this: *J. Mater. Chem. A*, 2013, **1**, 8665

Junshe Zhang,[a] Ayeong Byeon[a] and Jae W. Lee*[ab]

This work addresses the derivation of active electrocatalysts using carbon dioxide (CO_2) as a carbon source. CO_2 is converted to boron-doped porous carbon (B-PC) with sodium borohydride as a reduction agent at ambient pressure and 500 °C. Further activation of the BPC using the thermal treatment in the presence of $NaBH_4$ greatly enhances its catalytic activity for oxygen reduction reaction (ORR). The treated B-PC has ORR activity comparable to a Pt-activated carbon (Pt-AC) catalyst but it shows better ORR selectivity. The improvement of electrocatalytic performance is not originated from the carbon morphology change but comes from the change of surface boron bonds with carbon atoms and the widened π state. The synthesis of B-PC from CO_2 under mild conditions and the application of the derived B-PC to the fuel cell electrode might be one feasible way of numerous sustainable CO_2 utilization practices.

Received 28th March 2013
Accepted 17th May 2013

DOI: 10.1039/c3ta11248a

www.rsc.org/MaterialsA

1 Introduction

The polymer electrolyte fuel cell (PEFC) is one of the very promising devices to convert chemical energy of fuels into electricity, because it has high energy efficiency and low environment impact.[1] However, PEFCs have not been prevalently employed due to the lack of hydrogen infrastructure, technical issues related to their performance and durability, and their high cost.

The catalysts, based on platinum (Pt) or its alloys, are by far the most expensive constituent of PEFCs. Thus, numerous efforts have been made to develop non-precious metals or even metal-free catalysts for oxygen reduction reaction (ORR) at the cathode,[2–9] which normally requires more Pt than hydrogen oxidation reactions at the anode. Among these metal-free catalysts, nitrogen (N)-doped or boron (B)-doped carbon materials, including mesoporous graphitic arrays, carbon nanotubes, and graphene, exhibit excellent electrocatalytic activity toward ORR and possess the advantages of low cost and long lifetime.[7–9]

Generally, N- or B-doped carbon catalysts are derived from organics that undergo pyrolysis at temperatures above 800 °C.[7] As a readily available carbon source, carbon dioxide (CO_2) can also be converted to carbon materials such as carbon nanotubes, diamond, graphene oxide, and nested fullerenes subject to extreme conversion conditions.[10–13]

In contrast, mild reaction conditions (1 atm. and below 500 °C) are employed to uniquely synthesize B-doped porous carbon (B-PC) from CO_2 reaction with sodium borohydride ($NaBH_4$).[14] Because boron atoms have linkages to carbon lattices and they facilitate the electron transfer,[7–9] the B-PC synthesized from CO_2 is sure to have electrocatalytic activity toward ORR. The present work unprecedentedly demonstrates the catalytic performance of the B-PC and shows how it can be significantly improved after it is subjected to $NaBH_4$ treatment. The treated boron-doped porous carbon (TB-PC) and Pt-AC have comparable activity for ORR but the former possesses higher selectivity than the latter. This finding may portend a new avenue for fabricating metal-free electrocatalysts for ORR.

2 Experimental

2.1 Materials

Argon (Ar) with a purity of >99.9% and carbon dioxide (CO_2) with a purity of >99.8% were purchased from Deokyang Co. Ltd. Oxygen (O_2) with a purity of >99.995% was supplied by Deokyang Co. Ltd. Methanol (CH_3OH) with a purity of 99.8% was purchased from Merck KGaA. Ethanol (CH_3CH_2OH) with a purity of 99.9% and sodium hydroxide (NaOH) were acquired from Fisher Scientific. Sodium borohydride ($NaBH_4$) with a purity of >99% was obtained from Fluka. Hydrochloric acid (37 wt% in water), Nafion® 117 solution (~5 wt% in a mixture of lower aliphatic alcohols and water), and platinum (20 wt% loading) on activated carbon (Pt-AC) were acquired from Sigma-Aldrich. All chemicals were used as received without further purification.

2.2 Preparation of porous carbon from CO_2

After loading *ca.* 1.24 g of $NaBH_4$ onto a 5 cm^3 alumina crucible boat (McDanel Advanced Ceramic Technologies), the boat was put into a horizontal quartz tube (Ø 25 mm) mounted inside a

[a]*Department of Chemical and Biomolecular Engineering, KAIST, 291 Daehak-ro, Yuseong-gu, Daejeon, 305-701, Korea. E-mail: jaewlee@kaist.ac.kr; Fax: +82-42-350-3910; Tel: +82-42-350-3940*

[b]*Department of Chemical Engineering, The City College of New York, 140th St and Convent Avenue, New York, NY 10031, USA*

furnace (GSL1100X, MTI Co.). Then, the quartz tube was heated to 500 °C from room temperature in 100 min, followed by maintaining this temperature for 2 h, and finally cooled down to room temperature under 0.1 MPa CO_2 (gauge pressure) with a flow rate of 76 cm^3 STP min^{-1}. The solid products from 4 repeated runs were collected and stored in a glass vial under ambient conditions. About 8.93 g of the solid product was put into a 250 cm^3 glass bottle (PYREX®), followed by addition of 200 cm^3 HCl solution (5 M). This resulted in a suspension of fine particles. After four days, the suspension was filtered, followed by washing the cake with deionized water. The cake was dispersed in 200 cm^3 D.I. water. Again, a suspension of fine particles formed and then was filtered after one day. The procedure of water-washing and dispersing the cake in 200 cm^3 D.I. water was repeated two more times. After that, the suspension was filtered and then the cake was washed with ethanol, followed by dispersing it in 200 cm^3 ethanol, which led to a fine particle suspension. After one day, the suspension was filtered. The cake was kept in the open air at room temperature for several hours and subsequently dried overnight in an oven at *ca.* 120 °C. The mass of the final product is *ca.* 0.604 g.

2.3 $NaBH_4$ treatment of porous carbon

The sodium borohydride solution was prepared by dissolving 0.118 g of $NaBH_4$ in 6 cm^3 ethanol. About 0.1 g of porous carbon was put into a 20 cm^3 glass vial, followed by adding 1.5 cm^3 $NaBH_4$ solution. The vial was left open for one or two days to allow evaporation of ethanol. The sample was loaded onto the alumina crucible boat, which was then put into a horizontal quartz tube mounted inside a furnace. After that, the quartz tube was heated to 100 °C from room temperature in 20 min, followed by maintaining this temperature for 1 h, and then heated to 850 °C in 75 min. The sample was kept at this temperature for 2 h. Finally it was cooled down to room temperature under 0.1 MPa Ar (gauge pressure) with a flow rate of 50 cm^3 STP min^{-1}. The resultant porous carbon was put into a 20 cm^3 glass vial, followed by adding 20 cm^3 HCl solution (5 M). It led to a suspension of fine particles. The suspension was placed in a closed vial for 5 days, after which black particulates precipitated and a clear supernatant was obtained. The liquid was withdrawn with a 10 cm^3 pipette, to which 20 cm^3 of D.I. water was added, followed by capping the vial. Again, a suspension formed, which precipitated after 1 day, resulting in a clear supernatant. The procedure of withdrawing the clear liquid and adding 20 cm^3 of D.I. water was repeated five more times, and finally 20 cm^3 of ethanol was used for washing. After the clear supernatant was withdrawn in the last washing step, the resultant particles were kept in an open vial for several hours and subsequently dried overnight in an oven at *ca.* 120 °C.

2.4 Characterization

High resolution transmission electron microscopy (TEM) images were obtained with a Tecnai G2 F30 (FEI) field emission microscope operating at 300 kV. The samples for TEM were prepared by drop-casting a suspension of porous carbon in ethanol on a copper grid and then drying them under ambient conditions. Powder X-ray diffraction (XRD) measurements were performed using a D/MAX-2500 X-ray (Rigaku) diffractometer for a 2θ range of 10 to 80° at a scan rate of 2 °min^{-1}, a step size of 0.02°, and using graphite monochromatic Cu Kα ($\lambda = 1.5406$ Å) radiation with a nickel filter. The tube current was 300 mA with a tube voltage of 40 kV. Raman spectra were obtained by using an HR800 Horiba Jobin Yvon Dispersive-Raman system equipped with a CCD detector and an Olympus BX41 microscope with a 50× objective lens. Samples were placed on a cover glass and excited with 514.5 nm Ar ion laser radiation. The spectrum was obtained by multiple spectral bandpasses between 100 and 4000 cm^{-1}. Scanning electron microscopy (SEM) images were obtained with a Magellan 400 (FEI) field emission microscope. X-ray photoelectron spectroscopy (XPS) data were acquired by using a MultiLab 2000 (Thermo) system equipped with Al Kα radiation ($h\nu = 1486.6$ eV) as a probe under a chamber pressure of 5×10^{-10} mbar. The analysis spot size was 500 μm. The spectra were referenced to a C1s peak at 284.5 eV.

2.5 Electrochemical analysis

Electrochemical measurements, including CV (cyclic voltammetry) and RDE (rotating disk electrode) voltammetry, were performed at room temperature using an RRDE-3A rotating ring disk electrode rotator (ALS). The Ag/AgCl and platinum wire served as the reference and counter electrodes, respectively. The working electrode is a glassy carbon disk electrode (3 mm diameter). Potentials at the working electrode were controlled through a CHI 600D analyzer (CH Instrument). To deposit the catalyst on the disk, inks were prepared by dispersing 5.0 mg of catalyst in 1.0 mL solution of water, methanol, and Nafion® with a volume ratio of 3 : 1 : 0.1 by ultrasonication for 10 min. Then 3.5 μL of the catalyst ink was loaded onto the polished carbon disk electrode and dried overnight in air. ORR (oxygen reduction reaction) were carried out in 1 M NaOH electrolyte saturated and protected by oxygen. At the start of each experiment, the electrolyte was bubbled with oxygen at a flow rate of 15 STP cm^3 min^{-1} for 30 min. A flow of oxygen was maintained over the electrolyte while recording CVs in order to ensure its continued O_2 saturation. The working electrode was cycled at least 3 times before data were recorded at a scan rate of 50 mV s^{-1}. For RDE measurements, the working electrode was scanned at a rate of 10 mV s^{-1} with different rotating speeds.

3 Results and discussion

The electrocatalytic performance of B-PCs supported on glass carbon (GC) toward ORR was evaluated by cyclic voltammetry (CV) in a solution of 1.0 M NaOH saturated with 1 atm. oxygen. As shown in Fig. 1a, within a potential region of 0 to −1.0 V (*vs.* Ag/AgCl), the cathodic currents maximize around −0.31 and −0.21 V for the pristine B-PC (PB-PC) and the treated B-PC (TB-PC), respectively. The peak potentials are 0.69 and 0.79 V if they are expressed by the standard reversible hydrogen electrode (RHE). These observations exhibit that the $NaBH_4$-treatment enhances the electrocatalytic activity of PC for ORR and provides better ORR performance than other electrode

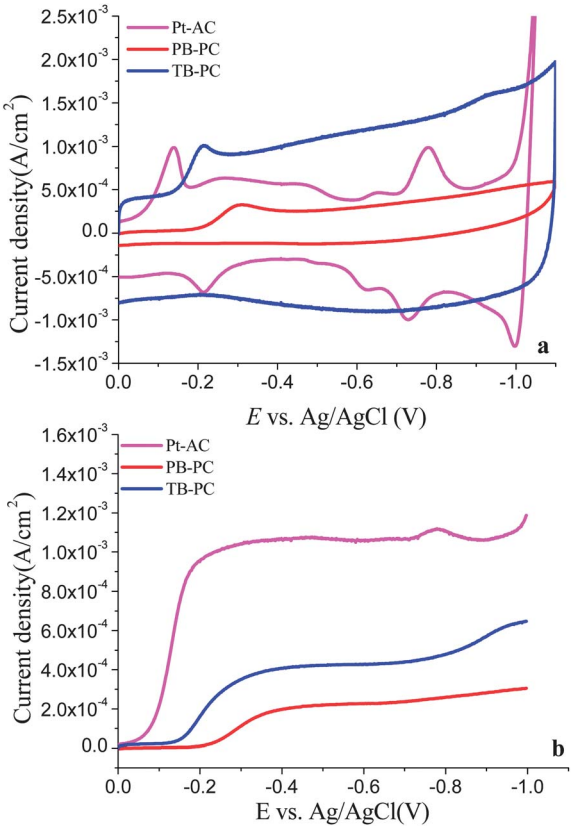

Fig. 1 Electrocatalytic performance of B-doped porous carbon/GC and Pt-AC/GC for oxygen reduction reaction in O_2-saturated 1.0 M NaOH solution: (a) cyclic voltammograms at a scan rate of 50 mV s^{-1}; (b) rotating disk electrode voltammograms with a rotating rate of 2500 rpm at a scan rate of 10 mV s^{-1}.

materials. For example, the peak potentials based on the RHE and the peak currents are 0.69 V and 0.815 mA cm^{-2} for B-doped (2.24 at.%) carbon nanotubes,[7c] and 0.67 V and 0.716 mA cm^{-2} for boron-doped graphene.[9] The maximum currents at the peak potentials are about 0.325 mA cm^{-2} for PB-PC and 1.02 mA cm^{-2} for TB-PC. A further examination of Fig. 1a reveals that the charging current (non-Faradaic current) is much larger for TB-PC (0.396 mA cm^{-2}) than that for PB-PC (0.042 mA cm^{-2}) as shown in Fig. 1a. After taking into account the charging current, the maximum current for TB-PC is twice as high as that for PB-PC. Similar patterns are also observed for the steady-state diffusion currents (Fig. 1b).

The onset potentials for ORR at PB-PC, TB-PC, and Pt (20 wt%)-AC electrodes are −0.15, −0.1, and −0.035 V, respectively (Fig. 1b). Unlike the Pt-AC/GC electrode, both PB-PC/GC and TB-PC/GC electrodes show a two-step process, with a second onset potential of around −0.62 V. The two-step behaviour was also reported for N-doped carbon nanotube/GC and B-doped graphene/GC electrodes.[2a,9] In addition, a well-defined limiting current cannot be identified on the steady-state voltammograms for Pt-AC/GC, PB-PC/GC, and TB-PC/GC electrodes as the potential approaches −1.0 V. This is attributed to the heterogeneous distribution of electrocatalytic sites, or the depth of O_2 penetration inside porous electrodes varying with the potential.[15]

To obtain more insight into ORR on the TB-PC/GC electrode, we performed rotating disk electrode (RDE) voltammetry in 1.0 M NaOH solution saturated with 1 atm. oxygen at a rotating rate range of 400 to 2500 rpm. As can be seen in Fig. 2a, both the charging current and the first onset potential are independent of rotating rates. However, the polarization curve in the second step becomes more inclined as the rotating rate increases, which is due to the same reason for the absence of well-defined limiting current at high overpotentials as mentioned above.

The transferred electron number (n) per oxygen molecule involved in ORR at the TB-PC/GC electrode was calculated from the Koutecky–Levich equation (eqn (1)):[16]

$$\frac{1}{I} = \frac{1}{I_K} + \frac{1}{I_d} = \frac{1}{nFAk(E)C_o^*} + \left(\frac{1}{0.62nFAD_O^{2/3}C_o^*\nu^{-1/6}}\right)\left(\frac{1}{\omega^{1/2}}\right) \quad (1)$$

$$\omega = 2\pi N/60 \quad (2)$$

in which I is the measured current (A) with the charging current correction (9.5 μA), I_K is the kinetic limiting current (A), I_d is the diffusion limiting current (A), n is the transferred electron number per oxygen molecule involved in ORR, F is the Faraday constant (96 485 C mol^{-1}), $k(E)$ is the electron-transfer rate constant (cm s^{-1}), E is the potential (V), A is the cross-sectional area of the GC electrode (7.07 × 10^{-2} cm^2), D_O is the diffusion coefficient of O_2 in 1.0 M NaOH (1.9 × 10^{-5} cm^2 s^{-1}),[17] C_O^* is the

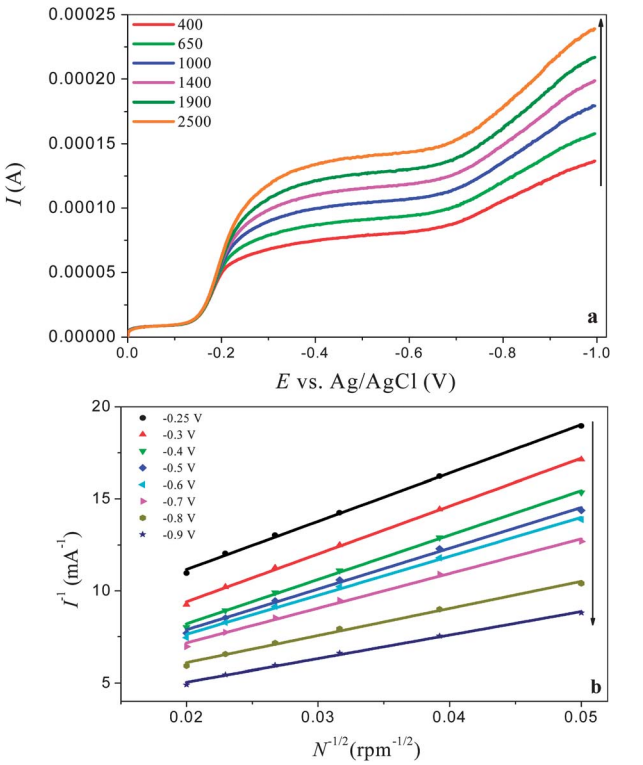

Fig. 2 (a) Rotating disk electrode (RDE) linear sweep voltammographs for the TB-PC/GC electrode in O_2-saturated 1.0 M NaOH solution at a scan rate of 10 mV s^{-1}; (b) Koutecky–Levich plots (I^{-1} *vs.* $N^{-1/2}$) for ORR on the TB-PC/GC electrode at different potentials.

bulk concentration of O_2 in 1.0 M NaOH (9.698×10^{-7} mol cm^{-3}),[18] ν is the kinetic viscosity of 1.0 M NaOH (1.087×10^{-2} cm^2 s^{-1}),[19] ω is the angular velocity of the disk (s^{-1}), and N is the rotating speed (rpm).

According to eqn (1), n can be obtained from the slope of I^{-1} *vs.* $N^{-1/2}$ plots (Fig. 2b). At a potential range of −0.25 to −0.6 V, the average transferred electron number is 2, and it is 3.3 at potentials between −0.7 and −0.9 V (Fig. 3a). Thus, the TB-PC/GC electrode exhibits a two-electron pathway at low overpotentials but a four-electron pathway at high overpotentials for the ORR. At potentials between −0.4 and −0.7 V, the intercept of the slope of I^{-1} *vs.* $N^{-1/2}$ plots does not change with respect to the potential, indicating that the electron transfer at the electrode surface might not be the rate-determining step as the rotating rate approaches infinity in the above potential range. Under this condition, other processes such as adsorption could be much slower than the charge transfer.

In addition to the excellent electrocatalytic performance for ORR, the TB-PC also has a good tolerance of methanol crossover, another main challenge faced by metal-based cathode catalysts in fuel cells. The chronoamperometric responses to methanol introduction into O_2-saturated 1.0 M NaOH solution for TB-PC and Pt-AC catalysts are presented in Fig. 3b. After introducing 1.0 cm^3 of CH_3OH, a sharp decrease in the current is observed for the Pt-AC catalyst, whereas a small but noticeable increase in the current is observed for the TB-PC catalyst. These results demonstrate that the TB-PC can act as a metal-free electrocatalyst for ORR with excellent activity and high tolerance to the crossover effect. To further understand the origin of electrocatalytic activity of boron-doped porous carbons, we carried out physical characterizations of both PB-PC and TB-PC.

X-ray photoelectron spectroscopy (XPS) provides chemical information of a surface, including the atomic composition and bonding state of elements. The surface atomic fractions of B, C, and O for TB-PC (PB-PC) are 4.13 (9.03), 84.92 (70.39), and 10.01 (19.47)%, respectively (Table 1). We used only $NaBH_4$ and CO_2 for the production of PB-PC and used Ar for the $NaBH_4$ treatment. Thus, N is not supposed to be involved in the above two steps. Most probably, N_2 in the air is adsorbed onto PB-PC in a vial or in a furnace which is not tightly sealed and may be involved in the reaction steps. In the XPS B1s spectra, two principal peaks at *ca.* 187.8 and 191.4 eV are observed for PB-PC (Fig. 4a), corresponding to B–C (B-I) and O–B–C (B-II) species of the carbon network into which boron atoms are incorporated,

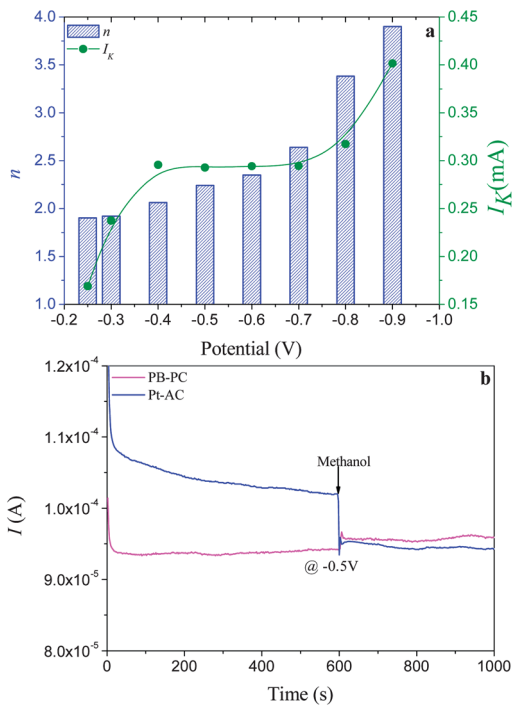

Fig. 3 (a) The transferred electron number and the kinetic limiting current at different potentials; (b) chronoamperometric response at −0.5 V in O_2-saturated 1.0 M NaOH solution on Pt-AC/GC and TB-PC/GC electrodes before and after introducing 1.0 cm^3 methanol.

Table 1 Surface elemental composition (atm.%)

	B	C	N	O
PB-PC	9.03	70.39	1.11	19.47
TB-PC	4.13	84.92	0.94	10.01

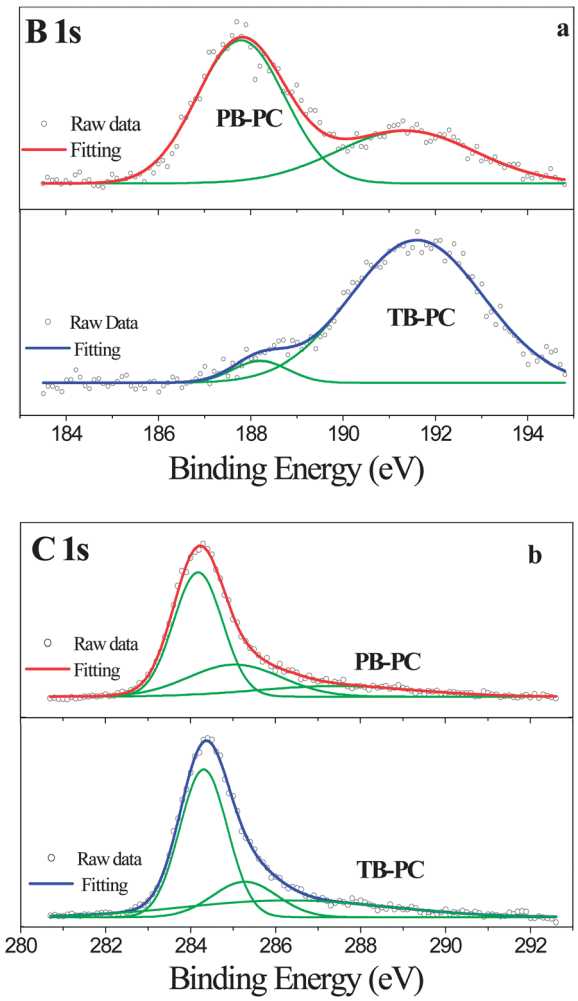

Fig. 4 (a) XPS B1s spectra PB-PC and TB-PC; (b) XPS C1s spectra PB-PC and TB-PC.

respectively. [9,20,21] The former is assigned to B_4C and the latter to BCO_2. Based on the area of fitted peaks, the surface concentration of B-I and B-II species is estimated to be 5.72 and 3.31 at.%, respectively.

For TB-PC, one distinct peak with a shoulder on the low binding-energy side is observed (Fig. 4a), which can be deconvoluted into two peaks at 188.2 and 191.6 eV. These two peaks are assigned to B_4C and BCO_2, respectively. A very notable observation is that the surface concentration of B-I species decreases significantly after the $NaBH_4$ treatment. Specifically, the surface concentration of B-I and B-II species in TB-PC is estimated to be 0.25 and 3.88 at.%, respectively. Thus, almost all of the B_4C species evolve into volatile compounds during the treatment but BCO_2 species is insensitive to the treatment.

In the XPS C1s spectra (Fig. 4b), a broadened peak that can be deconvoluted into three peaks at *ca.* 284.3, 285.1, and 287.4 eV is observed for PB-PC. The first peak is assigned to graphitic carbon (C–C sp^2). [7c,9,21,22] The last two peaks are assigned to B–C–O and C═O species, respectively. The peak related to B_4C (282.0 eV) [21] is not observed due to the low surface concentration. For TB-PC, the broadened peak can be deconvoluted into three peaks, centered at *ca.* 284.3, 285.3, and 286.3 eV. The last two peaks are assigned to B–C–O and C–O species, [23,24] respectively. Thus, it is inferred that C═O species also evolve into volatile compounds during the $NaBH_4$ treatment.

X-ray diffraction (XRD) is a non-destructive and well-established technique for studying the structure of carbon materials. For both PB-PC and TB-PC, a broad diffraction peak centered at *ca.* 23.5° is observed at a 2θ range of 10 to 30° in the XRD spectra shown in Fig. 5, indicating that the microstructure of porous carbon obtained from CO_2 reaction with $NaBH_4$ is amorphous. The amorphous feature is also revealed by the high-resolution transmission electron microscopy (HRTEM) images (Fig. 6).

Fig. 5 shows that TB-PC has some unknown small peaks at 35–65° 2θ. Because Na is not observed in the XPS spectra (Fig. 4), these are not related to the salts of Na_2CO_3 and $NaBO_2$ which are the byproduct salts from CO_2 reaction with $NaBH_4$ as shown in our previous work. [14] These peaks may be attributed to unknown boron carbides.

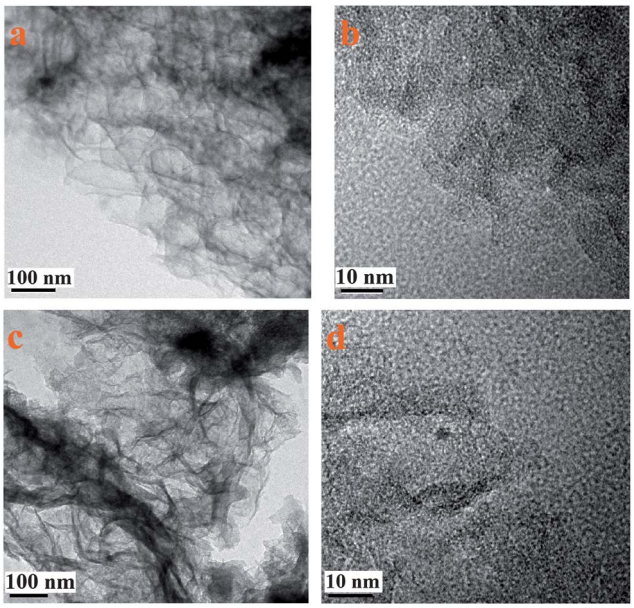

Fig. 6 High-resolution TEM images of PB-PC (a) and (b) and TB-PC (c) and (d).

Raman spectroscopy is another non-destructive and effective tool to determine the clustering of the sp^2 phase, disordered structure, and ration of sp^2 (graphite-like) to sp^3 (diamond-like) bonds. [25] The Raman spectra of PB-PC and TB-PC are shown in Fig. 7. For PB-PC, the two most pronounced peaks in the spectra are the D band at *ca.* 1366 cm^{-1} and the G band at *ca.* 1592 cm^{-1}. For TB-PC, the D band shifts to 1355 cm^{-1} and the G band shifts to 1584 cm^{-1}. According to Ferrari and Robertson, [25] the degree of amorphization of amorphous carbon decreases as the G band peak shifts to the lower wavenumber. Thus, TB-PC has a more ordered structure than PB-PC. For both PB-PC and TB-PC, a weak and broadened band is observed between 2250 and 3350 cm^{-1}, which is attributable to a combination of 2D, D + G, and 2G modes.

A further analysis of Raman spectra reveals that the I_D/I_G (the ratio of peak heights) is 0.66 and 0.93 for PB-PC and TB-PC,

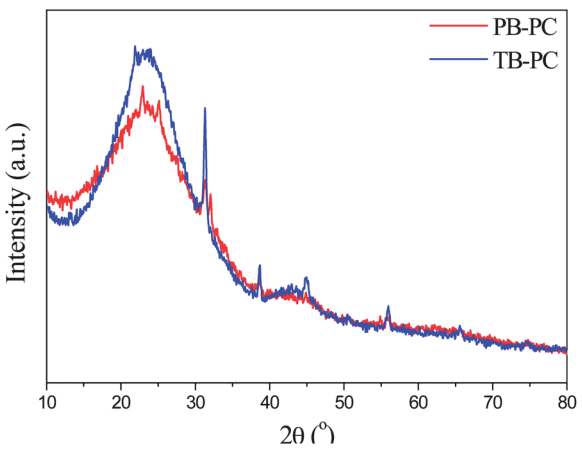

Fig. 5 XRD spectra for PB-TC and TB-PC.

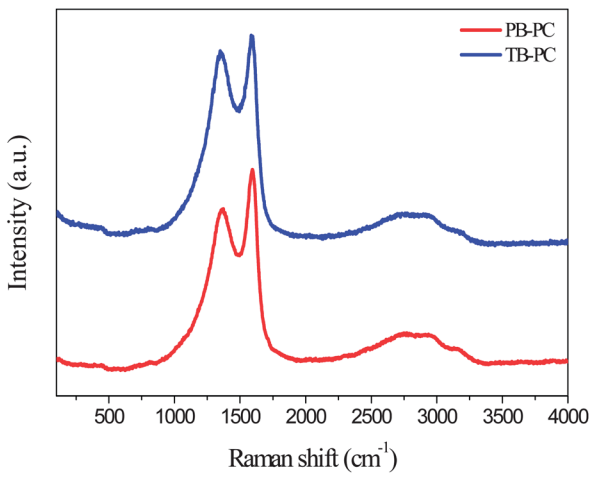

Fig. 7 Raman spectra for PB-PC and TB-PC.

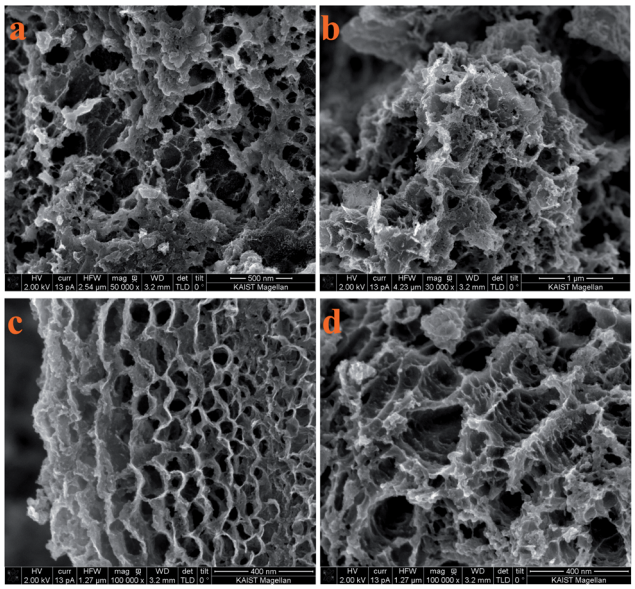

Fig. 8 SEM images of PB-PC (a) and (b) and TB-PC (c) and (d).

respectively. The relationship between the I_D/I_G and the average size of sp^2 carbon clusters (L_a) or the optical band gap (E_g) of amorphous carbon materials is proposed by Ferrari and Robertson.[25]

$$\frac{I_D}{I_G} = C'(\lambda){L_a}^2 = \frac{C''}{{E_g}^2} \quad (3)$$

where C' and C'' are constants.

According to eqn (3), the optical band gap of TB-PC is narrower than that of PB-TC. For amorphous carbon materials, the optical band gap is determined by the π states of the sp^2 sites.[26] The I_D/I_G ratio increases as the degree of amorphization decreases.[25] This is in line with the G band shift to the lower wavenumber as mentioned above. If the I_D/I_G ratio increases, the optical band gap (E_g) in eqn (3) reduces and the π band widens.[27] The reduced band gap energy and widened π state clearly enhance the oxygen reduction through facilitated electron transfer.

This result, together with the XPS analysis, clearly demonstrates that the $NaBH_4$ treatment not only affects the band structure but also alters the surface species. The treatment, however, seems to have little effect on the morphology of porous carbon, as evidenced by XRD analysis (Fig. 5), TEM images (Fig. 6) and scanning electron microscopy (SEM) images (Fig. 8). Thus, based on the XPS, XRD, HRTEM, Raman, and SEM results, it can be summarized that the improved electrocatalytic performance is due to widened π bands and more active sites generated from the decomposition of B_4C and C=O species.

4 Conclusions

We have demonstrated that the B-doped porous carbon obtained from CO_2 reaction with $NaBH_4$ can catalyze oxygen reduction reaction in alkaline solutions. Also, our observations have evidenced that the $NaBH_4$ treatment dramatically improves its electrocatalytic performance. The treatment leads to widened π bands and active sites arising from the decrease in the surface concentration of B_4C and C=O species. In addition, the results have exhibited that the oxygen reduction reaction on B-doped porous carbons occurs through two processes, a two-electron pathway at low overpotentials and a four-electron pathway at high overpotentials.

Acknowledgements

The authors are grateful for the financial support from the Korea CCS R & D Center funded by the Ministry of Science, ICT and Future Planning and the KAIST BK 21 program funded by the Ministry of Education.

Notes and references

1 R. Borup, J. Meyers, B. Pivovar, Y. S. Kim, R. Mukundan, N. Garland, D. Myers, M. Wilson, F. Garzon, D. Wood, P. Zelenay, K. More, K. Stroh, T. Zawodzinski, J. Boncella, J. E. McGrath, M. Inaba, K. Miyatake, M. Hori, K. Ota, Z. Ogumi, S. Miyata, A. Nishikata, Z. Siroma, Y. Uchimoto, K. Yasuda, K. I. Kimijima and N. Iwashita, *Chem. Rev.*, 2007, **107**, 3904.
2 (*a*) K. Gong, F. Du, Z. Xia, M. Durstock and L. M. Dai, *Science*, 2009, **323**, 760; (*b*) M. Lefèvre, E. Proietti, F. Jaouen and J. P. Dodelet, *Science*, 2009, **324**, 71; (*c*) G. Wu, K. L. More, C. M. Johnson and P. Zelenay, *Science*, 2011, **332**, 443.
3 R. Bashyam and P. Zelenay, *Nature*, 2006, **443**, 63.
4 P. H. Matter, L. Zhang and U. S. Ozkan, *J. Catal.*, 2006, **239**, 83.
5 R. Kothandaraman, V. Nallathambi, K. Artyushkova and S. C. Barton, *Appl. Catal., B*, 2009, **92**, 209.
6 F. Jaouen, E. Proietti, M. Lefèvre, R. Chenitz, J. P. Dodelet, G. Wu, H. T. Chung, C. M. Johnson and P. Zelenay, *Energy Environ. Sci.*, 2011, **4**, 114.
7 (*a*) R. Liu, D. Wu, X. Feng and K. Müllen, *Angew. Chem., Int. Ed.*, 2010, **49**, 2565; (*b*) S. Yang, X. Feng, X. Wang and K. L. Müllen, *Angew. Chem., Int. Ed.*, 2011, **50**, 5339; (*c*) L. Yang, S. Jiang, Y. Zhao, L. Zhu, S. Chen, X. Wang, Q. Wu, J. Ma, Y. Ma and Z. Hu, *Angew. Chem., Int. Ed.*, 2011, **50**, 7132.
8 L. Qu, Y. Liu, J. B. Baek and L. Dai, *ACS Nano*, 2010, **4**, 1321.
9 S. H. Sheng, H. L. Gao, W. J. Bao, F. B. Wang and X. H. Xia, *J. Mater. Chem.*, 2012, **22**, 390.
10 M. Motiei, Y. R. Hacohen, J. Calderon-Moreno and A. Gedanken, *J. Am. Chem. Soc.*, 2001, **123**, 8624.
11 Z. Lou, Q. Chen, W. Wang and Y. Zhang, *Carbon*, 2003, **41**, 3063.
12 Z. Lou, Q. Chen, Y. Zhang, W. Wang and Y. Qian, *J. Am. Chem. Soc.*, 2003, **125**, 9302.
13 J. Zhang, Y. Zhao, X. D. Guan, R. E. Stark, D. L. Akins and J. W. Lee, *J. Phys. Chem. C*, 2012, **116**, 2639.
14 J. Zhang and J. W. Lee, *Carbon*, 2013, **53**, 216.
15 S. L. Gojković, S. Gupta and R. F. Savinell, *J. Electroanal. Chem.*, 1999, **462**, 63.

16 A. J. Bard and L. Faulkner, *Electrochemical Methods: Fundamentals and Applications*, Wiley, New York, USA, 2001.
17 C. Zhang, F. R. F. Fan and A. J. Bard, *J. Am. Chem. Soc.*, 2009, **131**, 177.
18 P. M. Sipos, G. Hefter and P. M. May, *J. Chem. Eng. Data*, 2000, **45**, 613.
19 D. Trromans, *Ind. Eng. Chem. Res.*, 2000, **39**, 805.
20 I. Ozaki, N. Kimura, T. Anahara and A. Oya, *Carbon*, 2007, **45**, 1847.
21 B. Ottaviani, A. Derré, E. Grivei, O. A. M. Mohamoud, M. F. Guimon, S. Flandroisa and P. Delhaèsa, *J. Mater. Chem.*, 1998, **8**, 197.
22 T. Shirasaki, A. Derré, M. Ménétrier, A. Tressaud and S. Flandrrois, *Carbon*, 2000, **38**, 1461.
23 A. Stein, Z. Wang and M. A. Fierke, *Adv. Mater.*, 2009, **21**, 265.
24 T. C. Nagaiah, A. Bordoloi, M. D. Sánchez, M. Muhler and W. Schuhmann, *ChemSusChem*, 2012, **5**, 637.
25 C. Ferrari and J. Robertson, *Phys. Rev. B: Condens. Matter Mater. Phys.*, 2000, **61**, 14095.
26 J. Robertson and E. P. O'Reilly, *Phys. Rev. B: Condens. Matter Mater. Phys.*, 1987, **35**, 2946.
27 M. Chhowalla, J. Robertson, C. W. Chen, S. R. P. Silva, C. A. Davis, G. A. J. Amaratunga and W. I. Milne, *J. Appl. Phys.*, 1997, **81**, 139.